AGU PUBLICATIONS

JGR

Journal of Geophysical Research: Space Physics

RESEARCH ARTICLE

10.1002/2014JA020614

Key Points:

- Observing Kelvin-Helmholtz waves at the dawnside Mercury magnetopause
- Confirming a dawn-dusk asymmetry associated with the Kelvin-Helmholtz at Mercury
- Determine characteristics associated with Kelvin-Helmholtz waves

Correspondence to:
E. Liljeblad,
elilil@kth.se

Citation:
Liljeblad, E., T. Sundberg, T. Karlsson, and A. Kullen (2014), Statistical investigation of Kelvin-Helmholtz waves at the magnetopause of Mercury, *J. Geophys. Res. Space Physics*, *119*, doi:10.1002/2014JA020614.

Received 15 SEP 2014
Accepted 14 NOV 2014
Accepted article online 19 NOV 2014

Statistical investigation of Kelvin-Helmholtz waves at the magnetopause of Mercury

E. Liljeblad[1], T. Sundberg[2], T. Karlsson[1], and A. Kullen[1]

[1]Space and Plasma Physics, School of Electrical Engineering, Royal Institute of Technology, Stockholm, Sweden, [2]School of Physics and Astronomy, Queen Mary University of London, London, UK

Abstract A large study of Kelvin-Helmholtz (KH) waves at the magnetopause of Mercury covering 907 days of data from the MErcury Surface Space ENvironment GEochemistry Ranging spacecraft have resulted in 146 encounters of not only nonlinear KH waves but also linear surface waves, including the first observations of KH waves at the dawnside magnetopause. Most of the waves are in the nonlinear phase (90%) occur at the duskside magnetopause (93%), under northward magnetosheath magnetic field conditions (89%) and during greater magnetosheath B_z (23 nT) values than in general. The average period and amplitude is 30 $\pm$ 14 s and 14 $\pm$ 10 nT, respectively. Unlike duskside events, dawnside waves do not appear at the magnetopause flank (<6 magnetic local time). This is in agreement with previous observations and modeling results and possibly explained by finite Larmor radius effects and/or a lack of a large-scale laminar flow at the dawnside magnetopause boundary.

1. Introduction

It is known that the transfer of energy, momentum, and plasma from the solar wind to Earth's magnetosphere does not only take place through magnetic reconnection but also through other mechanisms such as the Kelvin-Helmholtz (KH) instability [e.g., *Chen and Kivelson*, 1993; *Hasegawa et al.*, 2004]. KH waves can develop at the boundary between two plasma regions with different velocities, and such a condition is met at the magnetopause of any planetary magnetosphere. The plasma transfer is believed to take place when the KH waves become nonlinear and form rolled-up vortices.

KH waves have so far been observed at the magnetopause of Earth [e.g., *Chen and Kivelson*, 1993; *Fairfield et al.*, 2000; *Hasegawa et al.*, 2004], Saturn [*Masters et al.*, 2009, 2010] and Mercury [*Slavin et al.*, 2008; *Boardsen et al.*, 2010; *Sundberg et al.*, 2010, 2012]. The study of KH waves at Earth is more extensive than at Mercury, where only a few case studies exist. Moreover; KH waves have been observed at both the dawnside and duskside terrestrial magnetopause [e.g., *Chen and Kivelson*, 1993; *Hasegawa et al.*, 2006], whereas at Mercury only duskside waves have so far been reported [*Slavin et al.*, 2008; *Boardsen et al.*, 2010; *Sundberg et al.*, 2010, 2012]. Many authors have suggested that the asymmetry between the duskside and dawnside magnetopause is mainly due to finite Larmor radius (FLR) effects [e.g., *Nagano*, 1979; *Glassmeier and Espley*, 2006; *Nakamura et al.*, 2010; *Sundberg et al.*, 2010; *Paral and Rankin*, 2013]. The influence of the ion gyromotion on KH wave growth has been studied both by a FLR modified MHD approach [e.g., *Nagano*, 1979; *Glassmeier and Espley*, 2006; *Sundberg et al.*, 2010] and by fully kinetic or global kinetic hybrid simulations [e.g., *Nakamura et al.*, 2010; *Paral and Rankin*, 2013]. The FLR modified MHD approach concerns how the gyroviscous pressure of the ions affects the wave growth. As the vorticity of the magnetopause flow shear and the ion gyromotion are oppositely directed at the dusk flank but coincide on the dawn flank, the growth rates on the two flanks will be affected differently. Some authors have suggested that this will make the dawnside more unstable than the duskside [e.g., *Nagano*, 1979; *Sundberg et al.*, 2010], while others have predicted the opposite [e.g., *Glassmeier and Espley*, 2006]. The fully kinetic simulation on a Mercury-like ion-kinetic scale performed by *Nakamura et al.* [2010] has shown that as the convection electric field is directed in toward the magnetopause on the duskside and out from the magnetopause on the dawnside, the ion gyroradius becomes reduced on the duskside and enhanced on the dawnside, resulting in a broader velocity shear region at the dawnside compared to the duskside. As the growth rate of the KH waves depends on the thickness of the shear layer, the duskside is predicted to be more unstable to the KH instability than the dawnside. The few existing observations of KH waves at Mercury indicate the duskside

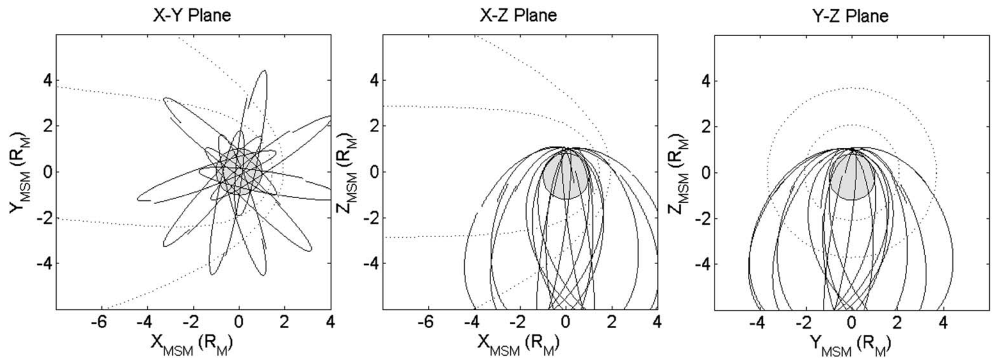

Figure 1. Nine orbits of MESSENGER during 29 March 2011 to 25 June 2011. MESSENGER returns to its original orbit after approximately 88 days.

flank to be the preferred location of KH waves at Mercury. However, a comprehensive statistical study of KH events at the magnetopause of Mercury is still missing.

The direction of the interplanetary magnetic field (IMF) is important for the development of KH waves. Observations of KH waves at the terrestrial magnetopause have typically shown a northward IMF [e.g., *Fairfield et al.*, 2000; *Ivchenko et al.*, 2000; *Nykyri and Otto*, 2001; *Hasegawa et al.*, 2006]. Even most of the few observed KH waves at the magnetopause of Mercury appeared during northward IMF [*Slavin et al.*, 2008; *Boardsen et al.*, 2010; *Sundberg et al.*, 2010, 2012].

The case studies of KH waves at Mercury by *Boardsen et al.* [2010] and *Sundberg et al.* [2012] indicate a period of 10–20 s. Note that both studies only cover events where the KH waves have become nonlinear. At Earth, however, the mean period for KH waves is considerably larger and lies in the interval of 2–5 min [e.g., *Fairfield et al.*, 2000; *Hasegawa et al.*, 2006].

In the present study we aim to do a systematic investigation of KH waves at the magnetopause of Mercury, using magnetic field data from the magnetometer instrument onboard the MErcury Surface Space ENvironment GEochemistry Ranging (MESSENGER) spacecraft. The main goal is to examine the location of KH waves on the Mercury magnetopause and to clarify a possible existence of a dawn-dusk asymmetry. The present work also includes a detailed examination of waveform, amplitude, period as well as magnetosheath, and solar wind conditions associated with or near in time to the KH waves.

2. Data Selection

The NASA MESSENGER spacecraft (MErcury Surface Space ENvironment GEochemistry Ranging) was inserted into orbit around Mercury in 18 March 2011, and has since then collected data from the surrounding space environment. To identify KH waves at Mercury's magnetopause, data from the magnetometer instrument have been used. The magnetometer can measure the magnetic field with an accuracy and resolution of 0.047 nT and 20 samples per second. For more details on the instrument, see *Anderson et al.* [2007].

The present study includes approximately 2.5 years of data between 24 March 2011 and 18 September 2013. During that time period, 907 days with data covering inbound and outbound magnetosphere crossings exist.

2.1. KH Selection

Figure 1 shows how MESSENGER's orbit varies over 88 days in MSM coordinates ($\hat{x}$ is directed from the center of the planet toward the Sun, $\hat{z}$ is pointing toward the magnetic dipole, and $\hat{y}$ completes the right-handed system). After that period of time Mercury has completed one orbit around the Sun, the spacecraft orbit has returned to its initial orientation, and MESSENGER has collected data from both the duskside and the dawnside magnetopause. MESSENGER's orbit never exceeds $z_{MSM} = 1\ R_M$, which as it turns out, will only have a small effect on the statistical study as most of the waves are encountered at $-0.4 < z < 0.4$. Moreover, MESSENGER did not traverse the magnetopause farther down the tail than $x_{MSM} = -2\ R_M$, making MESSENGER unable to collect possible KH data at the distant tail.

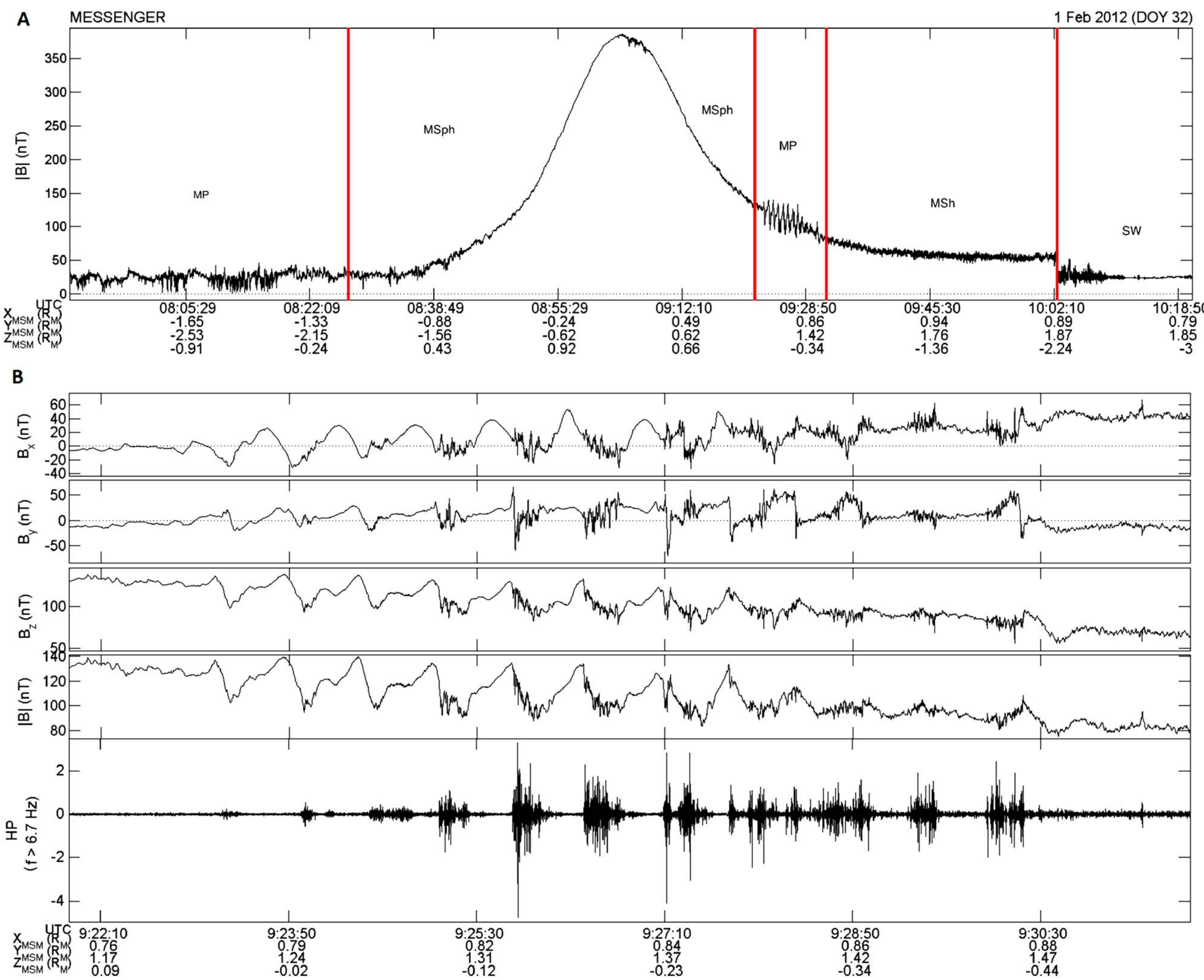

Figure 2. Example of typical duskside nonlinear KH waves at Mercury, showing MESSENGER's magnetic field data during an outbound encounter with Mercury's magnetopause. (a) Overview including the region of the nonlinear KH waves (KH) and traversal of Mercury's magnetosphere (MSph), magnetopause (MP), magnetosheath (MSh), and solar wind (SW). (b) A closer view of the KH waves marked in Figure 2a. The panels show, from top to bottom, the B_x, B_y, and B_z components of the magnetic field magnitude, the total magnetic field, and a high-pass filtering of the total magnetic field.

We begin by identifying all clear fluctuations, from the time period between 24 March 2011 and 18 September 2013, that appear close to or at the magnetopause. When MESSENGER is in the magnetopause region, the fluctuations in the magnetic field will show either an abrupt or gradual change in magnetic field signatures from the more varying and smaller $|B|$ magnetosheath magnetic field, to the less turbulent and larger $|B|$ magnetosphere magnetic field. We refer to these fluctuations at the magnetopause as candidate events. For those candidate events registered in 2011, the region of occurrence can be compared to the magnetopause identifications done by *Winslow et al.* [2013], and we can thus verify that all of these events appear at the magnetopause. In a second step, these candidate events are checked for three more criteria, allowing us to make a likely identification of KH waves: (1) Quasiperiodicity. (2) Consecutive magnetosphere and magnetosheath signatures during each wave period. (3) No indications of magnetopause motions or other active processes near the magnetopause, such as flux transfer events, ion cyclotron waves, or mirror waves.

An additional criterion concerning sawtooth signature in the magnetic field is used for the identification of nonlinear KH waves. The sawtooth signature appears due to a transition through a mixing region or vortex, containing both magnetosheath and magnetospheric plasma. This is registered as a gradual increase followed by an abrupt decrease in the magnetic field [e.g., *Hasegawa et al.*, 2004; *Fairfield et al.*, 2007]. An example of KH waves that have already developed beyond the linear stage is shown in Figure 2. Figure 2a

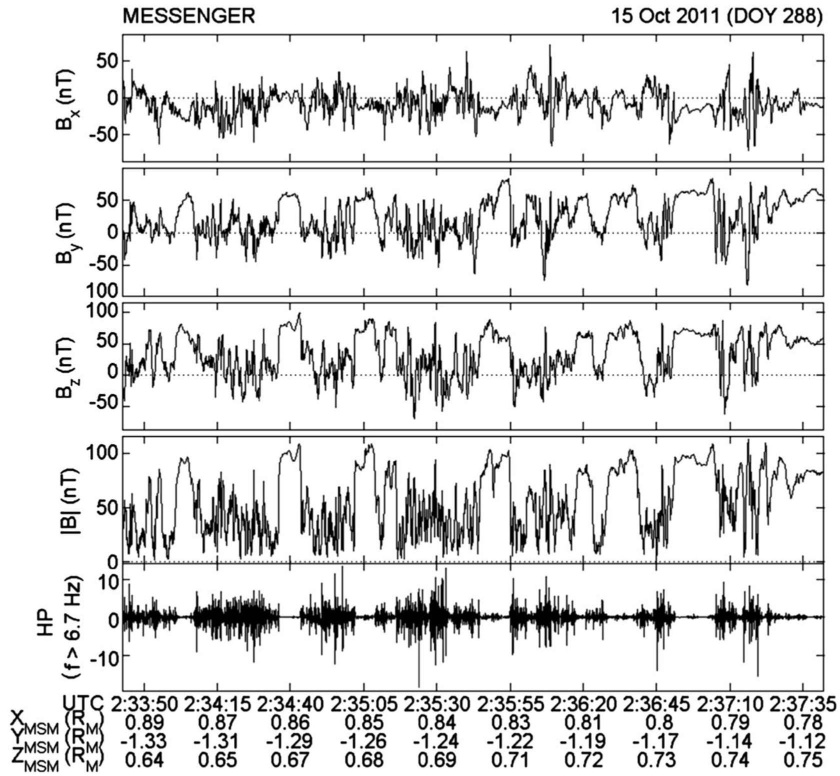

Figure 3. Example of linear waves at Mercury. The panels follow the same format as Figure 2b.

shows the overview of an entire passage on 1 February 2012, through regions of magnetosheath (MSh), magnetosphere (MSph), magnetopause (MP), nonlinear KH waves (KH), and solar wind (SW) magnetic field of Mercury, all marked with red lines. A closer view of the KH wave region is shown in Figure 2b, where the last panel shows the result of a high-pass filtering of the fourth panel. Note that this study does not treat a turbulent nonlinear stage in which the vortex structure is largely disturbed and a clear sawtooth signature no longer exists [*Nakamura et al.*, 2013].

Waves propagating along the magnetopause that lack a sawtooth structure in the magnetic field are referred to as linear waves. These waves are either initiated by the KH instability or by other dynamics in the magnetosheath, such as quasiperiodic reformation of a bow shock that is quasi-parallel and would be subject to KH wave growth as long as the wavelength is in the unstable domain. Linear waves are not associated with a mixing region, and we expect a box-like form in the magnetic field data. This form occurs when linear waves traverse MESSENGER, giving rise to a series of inbound and outbound crossings of the magnetopause where the magnetic field changes abruptly from the larger and calmer magnetospheric field to the lower and more turbulent magnetosheath field, or vice versa, as can be seen in the example of a linear wave in Figure 3. Visual inspection is used to determine whether the events are linear or nonlinear waves.

To determine whether the events fulfill the three different criteria listed above, the following analyses are performed for each candidate event:

The quasiperiodic behavior of criterion 1 is fulfilled if the candidate event shows a quasiperiodic structure with at least three wave peaks in the spacecraft reference frame (e.g., the KH event in Figure 2b shows nine such peaks).

Criterion 2 is satisfied when there is a distinct pattern of both fluctuating magnetosheath and more stable magnetospheric fields during each wave period. Such a clear periodic structure can be identified by a high-pass filtering the data, which removes the low-frequency components. In our analyses, we use a filter with a cutoff at 6.7 Hz. High-pass-filtered magnetic field data can be seen in Figure 2b, where the eight regions of strongly fluctuating magnetic field are associated with the magnetosheath, and the more smooth data in the period in between with the magnetosphere.

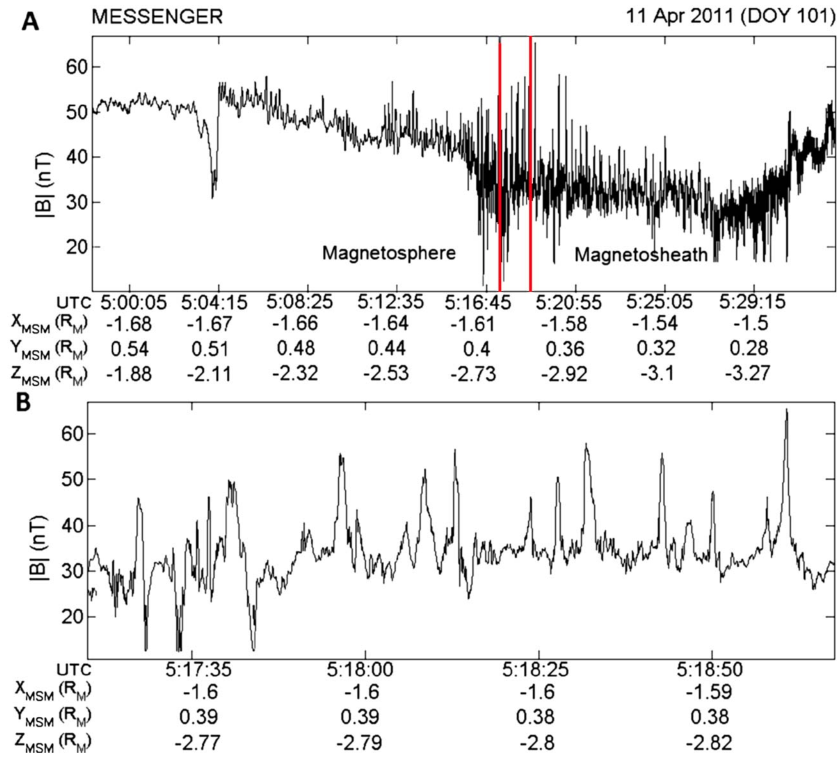

Figure 4. Magnetic field data of flux transfer events at Mercury from MESSENGER. (a) Overview of flux rope structures in magnetosphere and magnetosheath. The region of flux ropes is marked with red lines. (b) A closer view of the flux rope structures marked in Figure 4a.

Different types of dynamic features can occur regularly near or at the magnetopause, such as ion cyclotron waves (ICWs), magnetic mirror modes (MMs), flux transfer events (FTEs), and magnetopause fluctuations. In order to fulfill criterion 3, events exhibiting signatures of these waves must be excluded from the candidate event list. In total 41 events was removed from the candidate event list, where 20 of these were classified as magnetopause fluctuations, 13 as FTE, 8 as MM, and none as ICW.

The ICW-associated magnetic field is approximately perpendicular to the background magnetic field. Structures of nonlinear KH waves or linear waves, however, are generally seen in both parallel and perpendicular background magnetic field components. In a first step, possible ICWs are therefore identified by their wave direction: for those waves that show clear magnetic field structures only perpendicular to the background magnetic field, the gyroperiod $\left(T = \frac{2\pi m}{|q|B}\right)$ for Na^+ is calculated using the average magnetic field over the region of the waves. The Na^+ ion is chosen for analysis for two reasons: it is the most abundant exospheric ion component at Mercury [e.g., *Zurbuchen et al.*, 2011], and it is heavier and shows larger periods (more similar to KH wave periods) in the magnetic field than the very abundant ion H^+ does. The analysis showed that the gyroperiod associated with each candidate KH event was at least 2 times larger (on average 12 times larger) than the period for the candidate KH event, and therefore, none of the candidate events was removed from the list.

The MMs do not have a steep sawtooth-like structure. They can therefore be similar to linear waves, which have not yet developed the vortex-like KH wave structure. There are observations of MM appearing near the magnetopause, but so far, no evidence of them occurring at the magnetopause [e.g., *Soucek et al.*, 2008]. Even though it is unlikely that MM occur at the magnetopause, we still need to check characteristics and surrounding data to be certain that our candidate events are not MM: one measurable characteristic of MM is their magnetic field orientation, which is almost parallel to the background magnetic field [e.g., *McKean et al.*, 1992]. This characteristic is first checked for all linear waves. For those waves that do not show clear magnetic field structures perpendicular to the background magnetic field, the state of the bow shock is investigated. When the bow shock is quasi-perpendicular, temperature anisotropies are created when the solar wind impinges on the magnetic field of Mercury, making it more likely for MM to develop

Table 1. Average of Location Probability, Wave Form, Period, Amplitude, Solar Wind (SW) and Magnetosheath (MSh) Magnetic Field for All, Dusk and Dawn, Linear Waves, and Nonlinear KH Waves

	All KH	Nonlinear	Linear	Dusk	Dawn	Dusk (Nonlinear/Linear)	Dawn (Nonlinear/Linear)
Location (%)				95	5		
Nonlinear (%)	90			96	4		
Linear (%)	10			67	33		
Period (s)	30 ±14	30 ±14	26 ±10	30 ±14	31 ±11	30 ± 14/ 27 ± 11	38 ± 9/ 25 ± 9
Amplitude (nT)	14 ±10	12 ±7	25 ±19	13 ±8	30 ±16	12 ±7/ 18 ±18	20 ±14/ 39 ±13
SW $\|B\|$ (nT)	20	20	18	20	17	20/20	21/13
SW B_x (nT)	5.6	6.0	2.5	5.9	0.39	6.4/−0.22	−4.1/8.1
SW B_y (nT)	−0.87	−0.73	−2.1	−1.3	−0.0054	−1.2/−2.5	11/−1.3
SW B_z (nT)	3.4	3.5	2.4	3.6	0.062	3.6/3.3	0.78/0.48
MSh $\|B\|$ (nT)	37	37	36	37	29	37/44	40/18
MSh B_x (nT)	8.2	8.6	4.8	8.2	9.2	8.7/1.8	7.6/11
MSh B_y (nT)	−0.27	0.54	−7.4	−1.1	11	−0.29/−11	21/0
MSh B_z (nT)	23	23	22	24	11	23/31	19/3.8
MSh $B_x > 0$ (%)	65	66	60	65	70	66/50	60/80
MSh $B_y > 0$ (%)	48	49	40	46	80	47/30	100/60
MSh $B_z > 0$ (%)	89	89	87	90	70	90/90	60/80

[e.g., *Czaykowska et al.*, 1998]. Those candidate events showing a quasi-parallel bow shock are therefore not removed from the candidate list.

FTE have characteristic flux rope structures that can resemble the typical sawtooth wave form of unstable KH waves. However, they have more irregular and sharp peaks (e.g., the FTE shown in Figure 4 studied by *Slavin et al.* [2012]). Such FTE are removed by visual inspection.

Magnetopause oscillations due to fluctuations in the magnetosheath dynamic pressure can also look similar to linear waves. Here we separate them by looking at the normal direction of magnetopause crossings

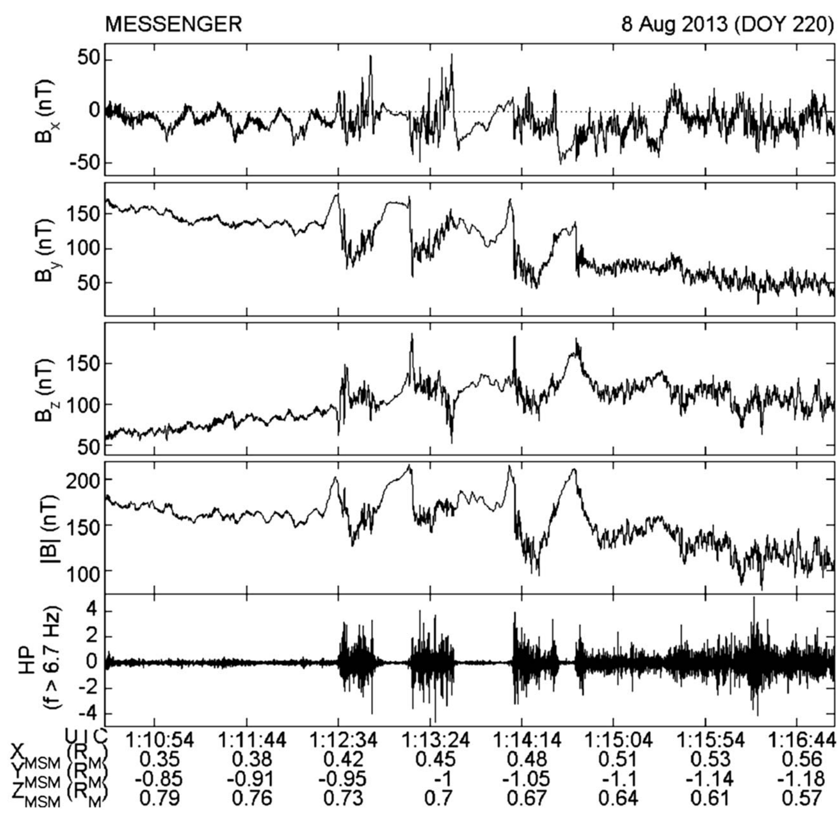

Figure 5. Example of dawnside nonlinear KH waves at Mercury. The panels follow the same format as Figure 2b.

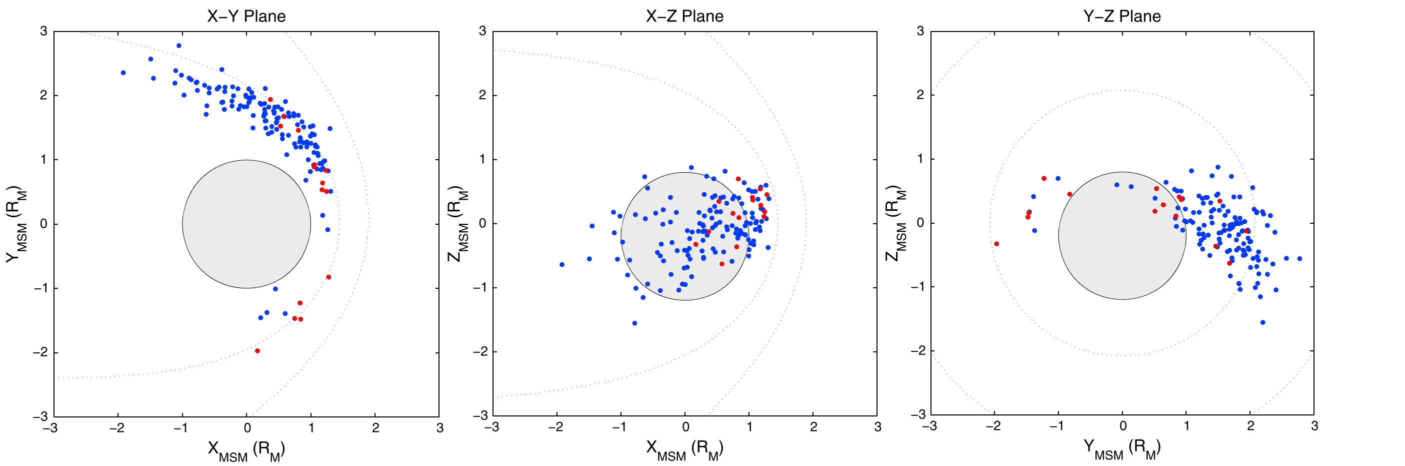

Figure 6. Positions of linear waves (red) and nonlinear KH waves (blue) around Mercury. Inner and outer dashed lines are approximated magnetopause and bow shocks, respectively.

of these waves: for a linear wave train, we expect the magnetopause normal to vary systematically between inbound and outbound crossings of the magnetopause [e.g., *Fairfield et al.*, 2000], whereas when the magnetopause move back and forth we expect the normal direction to be fairly unchanged. The magnetopause normal direction was determined with the minimum variance method. Hence, if we see a clear systematic change in the normal directions for the majority of the inbound and outbound crossings of the wave train, the event will not be removed from the candidate list.

The selection process has resulted in 146 events, fulfilling all three criteria listed above. One hundred thirty-one of these also satisfied the sawtooth criterion and are further on referred to as nonlinear KH waves, while the remaining 15 cases are referred to as linear waves.

2.2. Solar Wind and Magnetosheath Data Selection

Solar wind and magnetosheath conditions associated with the nonlinear KH waves and linear waves are also studied. The solar wind data for these events are selected by taking the average magnetic field of the solar wind excursion nearest in time to the waves. The average is taken over at least a 1 h period, depending on how much clearly identified solar wind data exist at that time. The magnetosheath magnetic field values are calculated by taking the average of the entire magnetosheath excursion nearest in time to the detection of the waves.

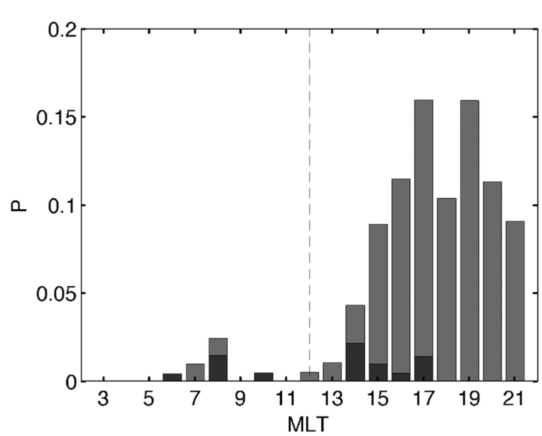

Figure 7. Positions of linear waves (dark grey) and nonlinear KH waves (light grey) around Mercury versus MLT, normalized with respect to the number of times MESSENGER traverses the magnetopause. The dashed line marks the subsolar point in this and subsequent figures.

For comparison with solar wind and magnetosheath conditions associated with the nonlinear KH waves and linear waves, 146 regions of data from solar wind and magnetosheath traversals are randomly selected from the set of 907 days of data, with the same averaging procedure as above.

3. Results

Average characteristics of the 146 events selected from the set of 907 days of data are summarized in Table 1. These include location, wave form, period, amplitude, and characteristics of solar wind and magnetosheath magnetic field data. The database includes the first documented KH waves on the dawnside magnetopause of Mercury. Examples of dawnside and duskside KH waves can be seen in Figures 5 and 2, respectively.

3.1. Location

Figure 6 shows the location of each nonlinear KH and linear event defined as the position of

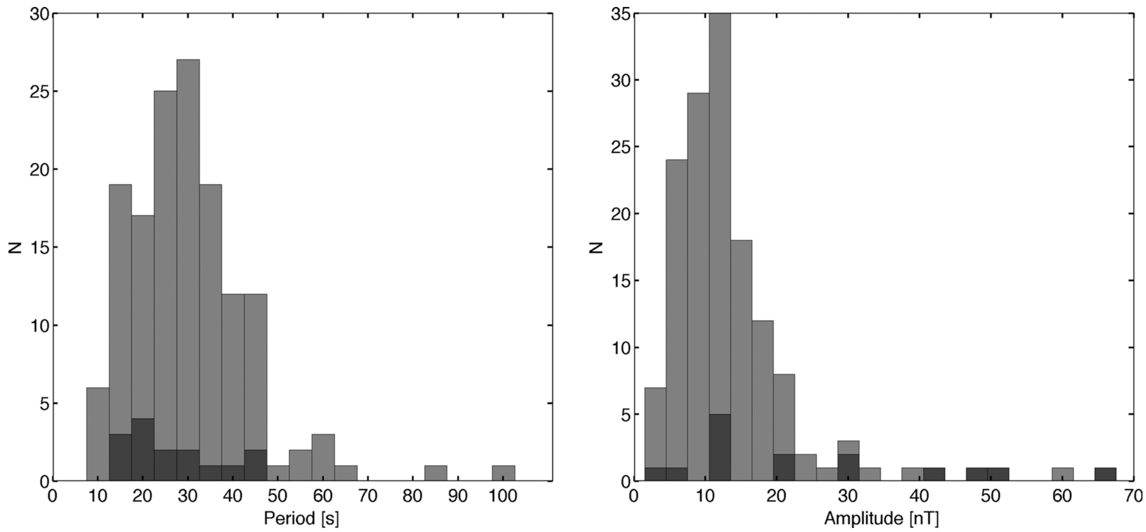

Figure 8. Period and amplitude for linear waves and nonlinear KH waves (light grey), with linear waves marked with (dark grey).

the spacecraft in the middle of the event, projected into three different planes in MSM coordinates. Linear waves and nonlinear KH waves are marked with red and blue, respectively. From Figure 6 it is clear that most of the waves, particularly nonlinear ones, are encountered at the duskside magnetopause but that a few waves are encountered also on the dawnside.

The linear waves are more evenly spread out at both sides of the magnetopause but are not encountered at the duskside distant tail like the nonlinear KH waves are. Taking into account that MESSENGER does not traverse the magnetopause farther down the distant tail than x_{MSM} =-2 R_M, the maximum occurrence probability of the duskside and dawnside waves is at 17–19 magnetic local time (MLT) and 8 MLT, respectively. This can be seen in Figure 7, showing the probability of observing KH waves at a certain MLT (i.e., the number of KH events has been normalized with respect to the number of times MESSENGER traverses the magnetopause) of linear waves (dark grey) and nonlinear KH waves (light grey). Moreover, from Figure 6 it can be seen that the large majority of the waves are encountered within $z_{MSM} = \pm 1$ R_M of the equatorial plane.

3.2. Wave Characteristics

The waves are characterized by wave form (linear or nonlinear), period, and amplitude. We define the period for each nonlinear KH and linear event as the mean of the time between consecutive minimum in the magnetic field in the direction of the mean magnetic field, referred to as the field-aligned direction. The

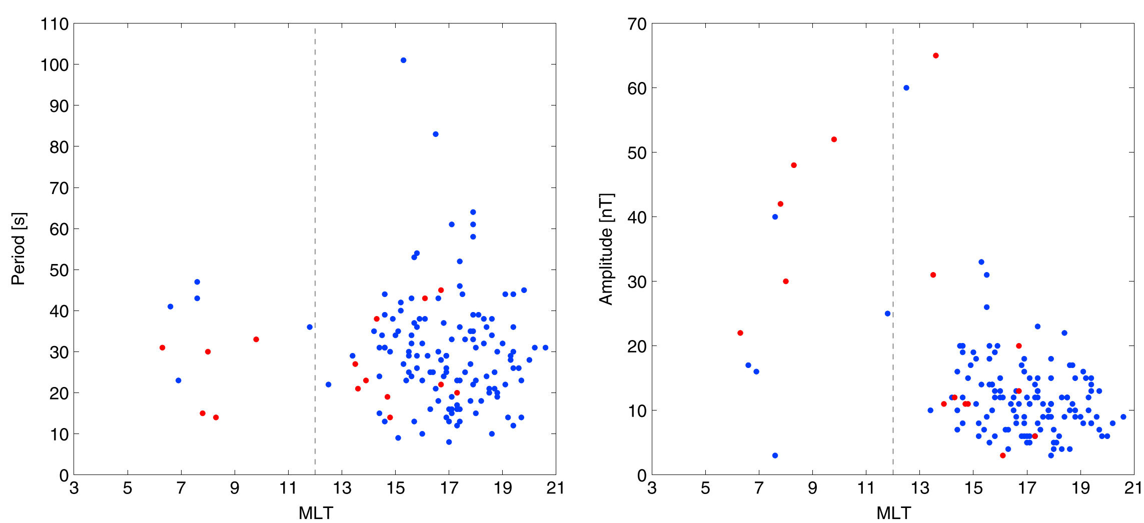

Figure 9. Period and amplitude for linear waves (red) and nonlinear KH waves (blue) versus MLT.

Table 2. Average of $|B|$, B_x, B_y, and B_z for 146 Randomly Selected Data From Solar Wind and Magnetosheath Regions

	Solar Wind	Magnetosheath
$\|B\|$ (nT)	18 ± 9	36 ± 21
B_x (nT)	3.6 ± 14	2.1 ± 19
B_y (nT)	-0.94 ± 12	0.28 ± 29
B_z (nT)	-0.047 ± 8	2.6 ± 24
$B_x > 0$ (%)		53
$B_y > 0$ (%)		51
$B_z > 0$ (%)		52

magnetic field amplitude, also in the field-aligned direction, is determined by the mean of the magnetic field for consecutive maximum minus the mean of the magnetic field over the whole wave packet.

Of all 146 waves, 90% are nonlinear KH waves according to our definition. On the duskside and dawnside 93% and 50% are nonlinear, respectively. Figure 8 shows a histogram of the period and amplitude of nonlinear KH waves (light grey) and linear waves (dark grey) in the spacecraft reference frame. The mean period for all waves (including standard deviation) is 30 ± 14 s, and for nonlinear KH waves and linear waves 30 ± 14 s and 26 ± 10 s, respectively. In Figure 9, which shows the period and amplitude versus MLT for nonlinear KH waves (blue) and linear waves (red), it can be seen that there is a similar spread in wave period for dawnside and duskside waves.

The mean amplitude for all waves is 14 ± 10 nT, and specifically 12 ± 7 nT and 25 ± 19 nT for nonlinear KH waves and linear waves, respectively (see Table 1). In Figure 9 it can be seen that after approximately 14 MLT there is a change in the distribution of amplitudes. Earlier than 14 MLT there is a larger spread in amplitude, particularly for the linear waves. After 14 MLT the amplitudes are less spread out with a mean around 10 nT.

3.3. Solar Wind and Magnetosheath Characteristics

The characteristics of the solar wind and the magnetosheath magnetic field data have been studied around the time of the observation of the waves. In order to compare with average characteristics, a random subset of magnetic field data from solar wind and magnetosheath traversals has been selected. The solar wind data are, as described in section 2.2, taken as near in time as possible to the waves. However, there can still be several hours between the solar wind and the magnetopause traversals. The solar wind magnetic field data are therefore used only as an indication of the IMF condition during the events. The magnetosheath magnetic field data are, as described in section 2.2, averaged over the entire magnetosheath traversal. It takes MESSENGER around 20 min to 2 h to traverse the magnetosheath, during which the magnetosheath magnetic field, in general, does not show any larger changes that affect the average magnetic field. Moreover, the magnetosheath is in direct connection to the wave observations, making the magnetosheath data a

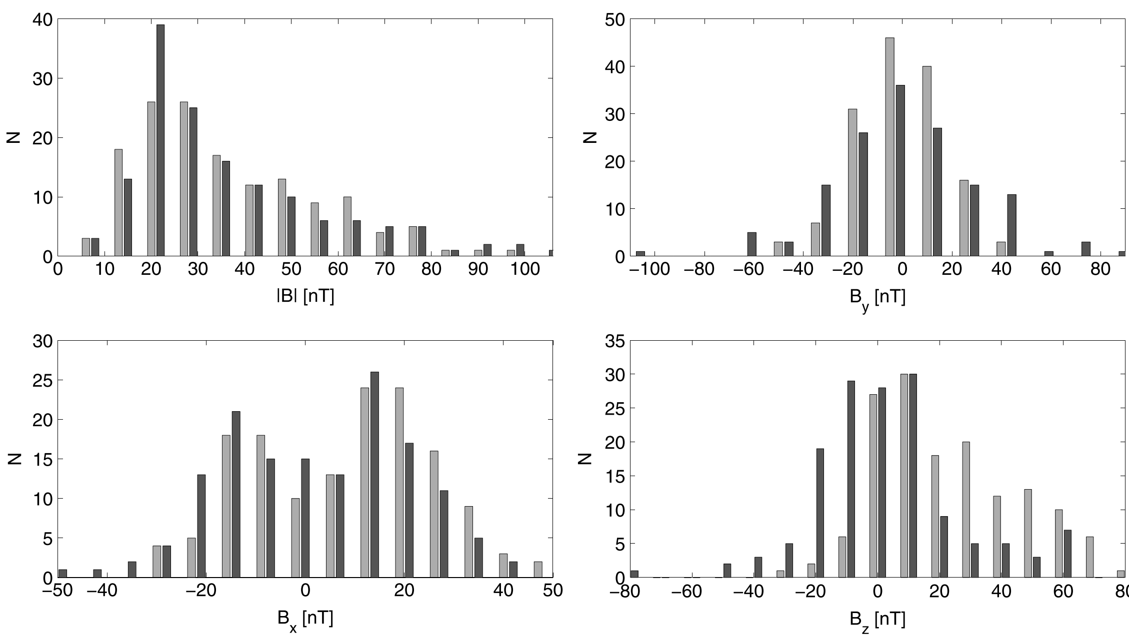

Figure 10. Magnetosheath $|B|$, B_x, B_y, and B_z for nonlinear KH waves and linear waves (light grey) and 146 randomly selected magnetosheath data (dark grey).

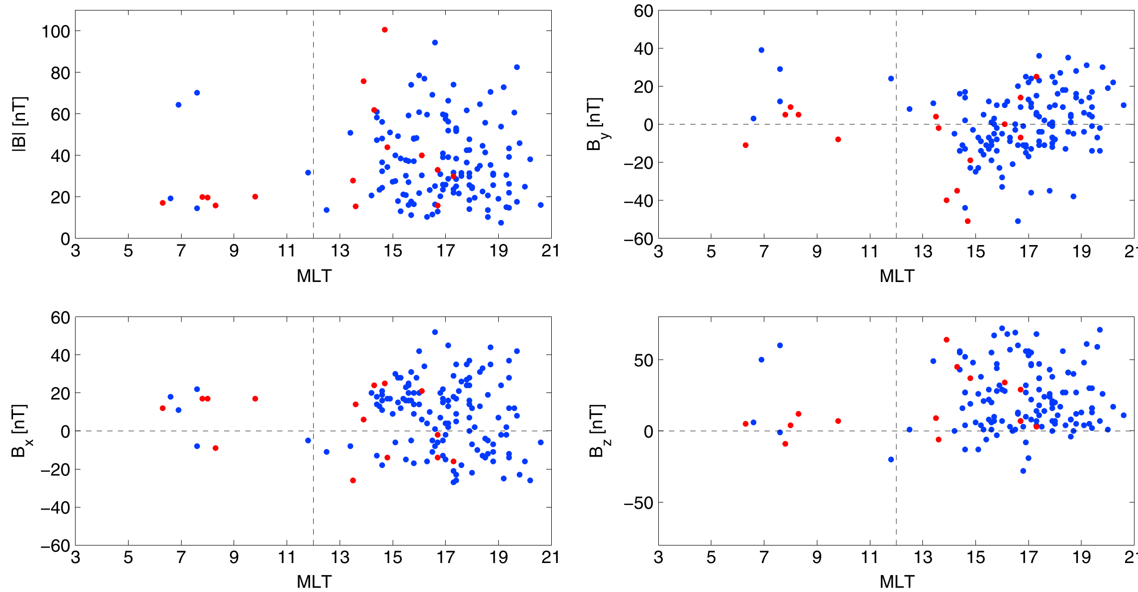

Figure 11. Magnetosheath $|B|$, B_x, B_y, and B_z for linear waves (red) and nonlinear KH waves (blue) versus MLT.

more relevant description of the magnetic field outside of the magnetopause. Average characteristics from the solar wind and magnetosheath magnetic field reference data points can be seen in Table 2.

The mean solar wind $|B|$ for all events is 20 nT and has approximately the same value for waves at both side of the magnetosphere and for linear waves and nonlinear KH waves (see Table 1). Moreover, the mean solar wind B_z for the reported waves is positive and slightly larger compared to the solar wind reference data set (see Table 2).

Figure 10 shows the histograms of the mean magnetosheath $|B|$, B_x, B_y, and B_z for nonlinear KH waves and linear waves (light grey), and the magnetosheath reference data (dark grey). The mean magnetosheath $|B|$ for all waves and the reference data set are 37 nT and 36 nT, respectively, and are also approximately equal in distribution. The distribution of the mean magnetosheath B_x for the reported waves and the reference data are similar, with slightly more positive B_x for the linear and nonlinear KH waves. Note also the typical double-peaked distribution associated with the solar wind B_x magnetic field. Figure 11, showing $|B|$, B_x, B_y, B_z versus MLT for linear waves (red), and nonlinear KH waves (blue), indicates that most waves, particularly dawnside ones, occur for positive B_x. Moreover, the majority of dawnside waves occur for weaker magnetosheath $|B|$ compared to waves at the duskside magnetopause. The percentage of positive B_x for the waves is 65 (see Table 1), compared to B_x for the reference data where 53% is positive. Hence, there is a small indication of the waves occurring more often for positive magnetosheath B_x, i.e., below the equatorial plane for the interplanetary current sheath. In Figure 10 we see that the B_y distribution is similar for the reported waves and the reference data set. B_z, however, differs considerably between the reported waves and the reference data set. It is clear from Figure 11 that the large majority of the observed waves, on both sides of the magnetosphere, occur for positive B_z. Eighty-nine percent of the B_z measurements for the waves are positive, while only 52% for the reference data is larger than zero. Moreover, the absolute value of the mean B_z is much larger for the reported waves than for magnetosheath data, in general (see Tables 1 and 2). Hence, there is an obvious relation between both the magnitude and sign of magnetosheath B_z and the occurrence of KH waves.

4. Discussion

A main result of this large statistical study is that nonlinear KH waves primarily occur at the duskside magnetopause. Unlike previous case studies on Mercury [*Slavin et al.*, 2008; *Boardsen et al.*, 2010; *Sundberg et al.*, 2010, 2012] we have, however, also observed a few events on the dawnside, making this the first recordings of dawnside KH waves at the magnetopause of Mercury. Moreover, the normalized distribution of KH waves in Figure 7 shows that the frequency of KH waves decreases at more distant tail regions (later than 19 MLT for duskside KH waves and earlier than 8 MLT for dawnside KH waves). This result is in contrast to previous KH wave observations at Earth, where the large majority of the nonlinear KH waves were identified tailward of the dawn-dusk terminator [e.g., *Hasegawa et al.*, 2006]. Our results show that there is not only a difference in KH occurrence frequency between Mercury and Earth regarding the dawn-dusk distribution but also regarding the distance from the dayside magnetopause.

The observation of nonlinear KH waves occurring predominantly at the duskside magnetopause is in agreement with predictions by several authors [e.g., *Glassmeier and Espley*, 2006; *Nakamura et al.*, 2010; *Paral and Rankin*, 2013], but in contrast to others [e.g., *Nagano*, 1979], suggesting the dawnside magnetopause to be more KH unstable. Simulations of the surroundings of Mercury have shown the duskside magnetopause to be more KH unstable [*Nakamura et al.*, 2010; *Paral and Rankin*, 2013]. This is explained by the FLR effect, or particularly by the convection electric field (CEF) effect on the ion gyroradius. The CEF extends (on the dawnside) or reduces (on the duskside) the gyroradii for ions crossing the shear layer. In turn, the ion gyroradii broaden the shear layer from an initial width, hence controlling the lower limit of the shear layer thickness. The thickness of the shear layer will in turn affect the linear growth rate of the KH waves, resulting in a larger growth rate on the duskside than on the dawnside magnetopause. Hence, if KH waves are able to develop at the dawnside, we would expect them to do so mainly when the dawnside shear layer is smaller, i.e., for a weaker CEF. This is partly supported by our results which show that the waves at the dawnside mainly occur for lower magnetosheath $|B|$ as compared to the duskside waves (see Figure 11).

A lower magnetosheath $|B|$, specifically for linear dawnside (and dayside) waves, can also be connected to the larger amplitudes for these waves as compared to the duskside waves. From Table 1 we see that the mean amplitude for all waves is 14 ± 10 nT and that the standard deviation is considerably smaller after 14 MLT than before (see Figure 9), i.e., the border is not at the subsolar point but rather 2 h later. Moreover, the amplitudes for the linear waves at the dawnside and near the subsolar point have a larger mean and are spread more widely than the amplitudes for those waves occurring at a later time. The amplitude is given by the absolute increase from lower to higher magnetic field values and does therefore also reflect the difference between magnetosheath and magnetospheric magnetic field values. A smaller magnetosheath magnetic field should thus result in a larger amplitude. Hence, we expect these linear dawnside and dayside waves to show larger amplitudes, in general. Looking at Figures 9 and 11, this is what we observe. The situation, however, is more complicated for nonlinear KH waves. These waves have enhanced magnetic field regions that contain a mix of both magnetosheath and magnetospheric magnetic fields, and a different wave structure compared to linear waves [e.g., *Fairfield et al.*, 2007]. When these waves pass MESSENGER, the largest magnetic fields will not correspond to clean magnetospheric magnetic fields, but rather to these mixing regions. Hence, it is more difficult to determine how the magnetosheath magnetic field will affect the amplitude for nonlinear KH waves.

Even though we do observe dawnside nonlinear KH waves and linear waves under certain magnetic field conditions, there is a total absence of dawnside KH waves at the flank. This observation may be connected to a result from the simulations of the solar wind interaction with Mercury by *Paral and Rankin* [2013], showing a lack of a steady magnetopause boundary at the dawn flank. The authors interpret this as a possible consequence from a Rayleigh-Taylor instability that breaks up the magnetopause boundary, which makes it highly difficult for dawnside KH waves to grow convectively along the flank. Another reason for not seeing KH waves at the dawnside flank could be related to the width of the velocity shear layer. On the dayside magnetopause we expect the shear layer and the magnetosheath to be smaller, as they will be compressed by the solar wind flow parallel to the magnetopause normal. On the flanks, however, the solar wind flow is almost perpendicular to the boundary normal and thus less able to compress the shear layer here than on the dayside magnetopause. This is also applicable to the dusk flank, but at the duskside the growth rate is large enough to overcome this inhibiting effect.

The direction of the IMF, approximated by B_z in the magnetosheath, shows a clear relation between large northward IMF and KH waves (see Figure 10). A large northward IMF component during KH wave occurrences has previously been reported at Earth [e.g., *Fairfield et al.*, 2000; *Hasegawa et al.*, 2006], and we can now establish that the situation is the same at the Mercury magnetosphere. Simulations by *Miura* [1995] have also shown the northward direction to be the most favorable IMF condition for the development of the KH instability. However, observations of nonlinear KH waves at Earth during southward IMF have indicated that KH waves can indeed develop under this condition but that the shape of these KH waves tend to be irregular and temporarily intermittent, making it more difficult to identify the KH waves during southward IMF [*Hwang et al.*, 2011]. Our results in this study show that any resolution of the IMF orientation effect on the KH instability must be valid for both the terrestrial and the Hermean magnetospheres.

At the duskside, most of the waves have reached their nonlinear stage already at around 15 MLT (see Figure 6). Hence, after existing for a while at the dayside magnetopause, the linear waves have quite quickly reached high enough amplitudes to become unstable and form rolled-up vortices, thus enabling the transfer of plasma from the magnetosheath to the magnetosphere. This means that KH waves will be an important factor in the interaction between the solar wind and the magnetosphere on Mercury, as it is on Earth under northward IMF conditions.

It can be difficult to separate whether the linear waves are exclusively driven by the KH instability, or if they are influenced also by other dynamic processes or pressure fluctuations that take place within the magnetosheath and/or the solar wind. One such source may be periodic reformations of the quasi-parallel bow shock, which can generate large quasiperiodic fluctuations in the magnetosheath magnetic field, as shown by *Sundberg et al.* [2013]. For this reason, we have chosen to call the quasiperiodic structures that are observed at or near the magnetopause, and lacking a sawtooth signature in the magnetic field, linear waves. These generally have the same characteristics in period, amplitude, and magnetosheath magnetic field as the nonlinear KH waves do. Thus, even though we cannot with certainty identify the source processes of each instance of these waves, the results of this study indicate that these are indeed linear KH waves, in general. More importantly, regardless of their initial generation, their location and their wave period indicate that these should be within the KH unstable regime, and thus, they will be subject to KH wave growth as they propagate along the magnetopause.

Finally, we want to point out that this is the first study where the period and magnetic amplitude of KH waves at Mercury can be determined more accurately. The mean period of the nonlinear KH waves in the spacecraft reference frame is 30 ± 14 s, i.e., at the same order of magnitude but slightly larger than 10–20 s as previously reported by *Boardsen et al.* [2010] and *Sundberg et al.* [2012]. The period for KH waves at Mercury is as expected much smaller than for KH waves at Earth, where the mean period is 2–5 min [e.g., *Kivelson and Chen*, 1995; *Fairfield et al.*, 2000; *Hasegawa et al.*, 2006]. Moreover, the period is slightly larger for nonlinear KH waves than for linear waves, which could possibly be explained by the merging of several waves at the flank where only nonlinear KH waves appear [e.g., *Nakamura and Fujimoto*, 2008]. Assuming a phase velocity of 150 km/s [*Boardsen et al.*, 2010] and a period of 30 s for the KH waves, the wavelength is 1.8 R_M. Furthermore, if we assume the velocity shear layer Δ to be as thick as the magnetopause, and assuming the magnetopause thickness to be 500 km [*Russell and Walker*, 1985], we get $k \cdot \Delta = 0.7$. This is almost equal to the maximum growth rate corresponding to $k \cdot \Delta = 0.8$, given by *Miura and Pritchett* [1982], indicating a reasonable order of magnitude of the KH wave periods.

5. Summary

A study on 907 days of magnetic field data from the MESSENGER spacecraft resulted in the finding of 131 nonlinear KH waves and 15 linear waves. The main results are given in the following list:

1. The large majority of the nonlinear KH waves are found at the duskside magnetopause between 15 and 19 MLT, confirming previous theoretical work predicting the duskside to be more KH unstable. New in this study is the discovery of KH waves also around noon and at dawn. In opposite to KH waves at dusk, dawnside KH waves do not occur farther down the flank than 6 MLT. Moreover, KH waves are more likely to occur sunward of the dusk-dawn terminator than behind it. As expected, the waves appear close to the equatorial plane (mainly within $z_{MSM} = \pm 1\ R_M$ to the equatorial plane).
2. The large majority of the reported waves are in their nonlinear state (90%). Linear waves are not found at the distant tail, whereas nonlinear KH waves occur as far down on the distant tail as MESSENGER allows us to investigate, i.e., to around $x_{MSM} = -2\ R_M$.
3. The mean period for all waves is 30 ± 14 s, and approximately equal for duskside and dawnside waves as well as for linear and nonlinear waves. The mean amplitude for all waves is 14 ± 10 nT. Moreover, the standard deviation of the amplitudes is much smaller at the duskside (after 14 MLT) than at the dawnside.
4. The estimated magnitude of the magnetosheath magnetic field connected to the reported waves is approximately equal to the general magnetosheath $|B|$. Eighty-nine percent of all linear waves and nonlinear KH waves, however, occur for positive magnetosheath B_z and larger absolute value compared to

average magnetosheath B_z, which is confirmed from previous KH studies at Earth. This means that KH waves at Mercury are a northward IMF phenomenon.

Future work should include analysis of the magnetopause of Mercury to find out whether we can observe signs of any large-scale instability breaking up the magnetopause at the dawnside, or if the width of the magnetosheath is different at the duskside and dawnside. It is expected that not only the direction of the IMF but also the solar wind velocity influences the occurrences of KH waves. Unfortunately, MESSENGER does not provide any velocity measurements. This can, however, be studied with the upcoming BepiColombo mission, the instrumentation of which will allow a more detailed investigation of KH waves at the Mercury magnetosphere. Moreover, a search for KH waves with Rosetta spacecraft may provide another example of KH waves where ion gyroradius effects can be important.

Acknowledgments
This work was partially supported by the Swedish National Space Board. The data for this paper are available at the NASA Planetary Data System: planetary plasma interactions node archive (http://pds-ppi.igpp.ucla.edu).

Yuming Wang thanks Scott Boardsen and another reviewer for their assistance in evaluating this paper.

References

Anderson, B. J., M. H. Acuña, D. A. Lohr, J. Scheifele, A. Raval, H. Korth, and J. A. Slavin (2007), The magnetometer instrument on MESSENGER, *Space Sci. Rev.*, *131*(1-4), 417–450.

Boardsen, S. A., T. Sundberg, J. A. Slavin, B. J. Anderson, H. Korth, S. C. Solomon, and L. G. Blomberg (2010), Observations of Kelvin-Helmholtz waves along the dusk-side boundary of Mercury's magnetosphere during MESSENGER's third flyby, *Geophys. Res. Lett.*, *37*, L12101, doi:10.1029/2010GL043606.

Chen, S.-H., and M. Kivelson (1993), On nonsinusoidal waves at the Earth's magnetopause, *Geophys. Res. Lett.*, *20*(23), 2699–2702.

Czaykowska, A., T. M. Bauer, R. A. Treumann, and W. Baumjohann (1998), Mirror waves downstream of the quasi-perpendicular bow shock, *J. Geophys. Res.*, *103*(A3), 4747–4753.

Fairfield, D., A. Otto, T. Mukai, S. Kokubun, R. Lepping, J. Steinberg, A. Lazarus, and T. Yamamoto (2000), Geotail observations of the Kelvin–Helmholtz instability at the equatorial magnetotail boundary for parallel northward fields, *J. Geophys. Res.*, *105*(A9), 21,159–21,173.

Fairfield, D., M. Kuznetsova, T. Mukai, T. Nagai, T. Gombosi, and A. Ridley (2007), Waves on the dusk flank boundary layer during very northward interplanetary magnetic field conditions: Observations and simulation, *J. Geophys. Res.*, *112*, A08206, doi:10.1029/2006JA012052.

Glassmeier, K.-H., and J. Espley (2006), Ulf waves in planetary magnetospheres, in *Magnetospheric ULF Waves: Synthesis and New Directions, Geophys. Monogr. Ser.*, vol. 169, edited by K. Takahashi, pp. 341–359, AGU, Washington, D. C.

Hasegawa, H., M. Fujimoto, T.-D. Phan, H. Reme, A. Balogh, M. Dunlop, C. Hashimoto, and R. TanDokoro (2004), Transport of solar wind into Earth's magnetosphere through rolled-up Kelvin–Helmholtz vortices, *Nature*, *430*(7001), 755–758.

Hasegawa, H., M. Fujimoto, K. Takagi, Y. Saito, T. Mukai, and H. Reme (2006), Single-spacecraft detection of rolled-up Kelvin-Helmholtz vortices at the flank magnetopause, *J. Geophys. Res.*, *111*, A09203, doi:10.1029/2006JA011728.

Hwang, K.-J., M. Kuznetsova, F. Sahraoui, M. Goldstein, E. Lee, and G. Parks (2011), Kelvin-Helmholtz waves under southward interplanetary magnetic field, *J. Geophys. Res.*, *116*, A08210, doi:10.1029/2011JA016596.

Ivchenko, N. V., D. Sibeck, K. Takahashi, and S. Kokubun (2000), A statistical study of the magnetosphere boundary crossings by the Geotail satellite, *Geophys. Res. Lett.*, *27*(18), 2881–2884.

Kivelson, M. G., and S.-H. Chen (1995), The magnetopause: Surface waves and instabilities and their possible dynamical consequences, in *Physics of the Magnetopause*, edited by P. Song, B. U. Ö. Sonnerup, and M. F. Thomsen, pp. 257–268, AGU, Washington, D. C.

Masters, A., N. Achilleos, C. Bertucci, M. Dougherty, S. Kanani, C. Arridge, H. McAndrews, and A. Coates (2009), Surface waves on Saturn's dawn flank magnetopause driven by the Kelvin–Helmholtz instability, *Planet. Space Sci.*, *57*(14), 1769–1778.

Masters, A., et al. (2010), Cassini observations of a Kelvin–Helmholtz vortex in Saturn's outer magnetosphere, *J. Geophys. Res.*, *115*, A07225, doi:10.1029/2010JA015351.

McKean, M., D. Winske, and S. Gary (1992), Mirror and ion cyclotron anisotropy instabilities in the magnetosheath, *J. Geophys. Res.*, *97*(A12), 19,421–19,432.

Miura, A. (1995), Dependence of the magnetopause Kelvin-Helmholtz instability on the orientation of the magnetosheath magnetic field, *Geophys. Res. Lett.*, *22*(21), 2993–2996.

Miura, A., and P. Pritchett (1982), Nonlocal stability analysis of the MHD Kelvin-Helmholtz instability in a compressible plasma, *J. Geophys. Res.*, *87*(A9), 7431–7444.

Nagano, H. (1979), Effect of finite ion Larmor radius on the Kelvin-Helmholtz instability of the magnetopause, *Planet. Space Sci.*, *27*(6), 881–884.

Nakamura, T., and M. Fujimoto (2008), Magnetic effects on the coalescence of Kelvin-Helmholtz vortices, *Phys. Rev. Lett.*, *101*(16), 165,002.

Nakamura, T., H. Hasegawa, and I. Shinohara (2010), Kinetic effects on the Kelvin-Helmholtz instability in ion-to-magnetohydrodynamic scale transverse velocity shear layers: Particle simulations, *Physics of Plasmas*, *17*(4), 42,119, doi:10.1063/1.3385445.

Nakamura, T., W. Daughton, H. Karimabadi, and S. Eriksson (2013), Three-dimensional dynamics of vortex-induced reconnection and comparison with THEMIS observations, *J. Geophys. Res. Space Physics*, *118*(9), 5742–5757, doi:10.1002/jgra.50547.

Nykyri, K., and A. Otto (2001), Plasma transport at the magnetospheric boundary due to reconnection in Kelvin-Helmholtz vortices, *Geophys. Res. Lett.*, *28*(18), 3565–3568.

Paral, J., and R. Rankin (2013), Dawn-dusk asymmetry in the Kelvin-Helmholtz instability at Mercury, *Nature Commun.*, *4*, 1645, doi:10.1038/ncomms2676.

Russell, C., and R. Walker (1985), Flux transfer events at Mercury, *J. Geophys. Res.*, *90*(A11), 11,067–11,074.

Slavin, J. A., et al. (2008), Mercury's magnetosphere after MESSENGER's first flyby, *Science*, *321*(5885), 85–89.

Slavin, J. A., et al. (2012), MESSENGER observations of a flux-transfer-event shower at Mercury, *J. Geophys. Res.*, *117*, A00M06, doi:10.1029/2012JA017926.

Soucek, J., E. Lucek, and I. Dandouras (2008), Properties of magnetosheath mirror modes observed by cluster and their response to changes in plasma parameters, *J. Geophys. Res.*, *113*, A04203, doi:10.1029/2007JA012649.

Sundberg, T., S. Boardsen, J. Slavin, L. G. Blomberg, and H. Korth (2010), The Kelvin-Helmholtz instability at Mercury: An assessment, *Planet. Space Sci.*, *58*(11), 1434–1441.

Sundberg, T., S. A. Boardsen, J. A. Slavin, B. J. Anderson, H. Korth, T. H. Zurbuchen, J. M. Raines, and S. C. Solomon (2012), MESSENGER orbital observations of large-amplitude Kelvin–Helmholtz waves at Mercury's magnetopause, *J. Geophys. Res.*, *117*, A04216, doi:10.1029/2011JA017268.

Sundberg, T., S. A. Boardsen, J. A. Slavin, V. M. Uritsky, B. J. Anderson, H. Korth, D. J. Gershman, J. M. Raines, T. H. Zurbuchen, and S. C. Solomon (2013), Cyclic reformation of a quasi-parallel bow shock at Mercury: Messenger observations, *J. Geophys. Res. Space Physics*, *118*, 6457–6464, doi:10.1002/jgra.50602.

Winslow, R. M., B. J. Anderson, C. L. Johnson, J. A. Slavin, H. Korth, M. E. Purucker, D. N. Baker, and S. C. Solomon (2013), Mercury's magnetopause and bow shock from MESSENGER Magnetometer observations, *J. Geophys. Res. Space Physics*, *118*, 2213–2227, doi:10.1002/jgra.50237.

Zurbuchen, T. H., et al. (2011), MESSENGER observations of the spatial distribution of planetary ions near Mercury, *Science*, *333*(6051), 1862–1865.

